

## Atomically resolved edges and kinks of NaCl islands on Cu(111): Experiment and theory

R. Bennewitz,<sup>1</sup> A. S. Foster,<sup>2</sup> L. N. Kantorovich,<sup>2</sup> M. Bammerlin,<sup>1</sup> Ch. Loppacher,<sup>1</sup> S. Schär,<sup>1</sup> M. Guggisberg,<sup>1</sup> E. Meyer,<sup>1</sup>  
and A. L. Shluger<sup>2</sup>

<sup>1</sup>*Department of Physics and Astronomy, University of Basel, Klingenbergstrasse 82, 4056 Basel, Switzerland*

<sup>2</sup>*Department of Physics and Astronomy, University College London, Gower Street, London WC1E 6BT, United Kingdom*

(Received 25 January 2000)

Atomically resolved dynamic force microscopy (DFM) images of step and kink sites of NaCl films grown on the Cu(111) surface are presented. Combining experimental results with an atomistic modeling of DFM imaging, we study the mechanism of contrast formation and extract more information about the tip and NaCl film structure. The experimental results and theoretical modeling systematically demonstrate the enhanced interaction of step and kink sites of one kind with the tip. This is explained by the enhanced gradient of the electrostatic potential at low-coordinated surface sites, and considerable displacements of the step edge and kink atoms from their sites due to the interaction with the tip upon approach. The theoretical analysis predicts that the silicon tip is effectively an insulator, and that the NaCl island cannot be thicker than two monolayers. We discuss the shape and chemical structure of the tip and the mechanism of damping during DFM imaging.

### I. INTRODUCTION

Recent progress in dynamic force microscopy (DFM) has opened avenues for understanding atomistic structure and properties of conducting and insulating surfaces.<sup>1,2</sup> However, DFM studies of insulators are still hampered by the charging and roughness of cleaved and/or cut and polished surfaces. Even in those few cases where atomic resolution has been achieved,<sup>3-6</sup> interpretation of images in terms of chemical identity of image features proved to be impossible.<sup>7</sup> Observation of unique image features which would demonstrate atomic resolution, such as surface point defects, has also been difficult and inconclusive.<sup>5,6</sup> This is partly due to the unknown structure of the very end of the tip, which determines the chemical interaction between the tip and surface, and hence the image contrast.<sup>3,8-11</sup> Another part of the problem is due to the difficulty in controlling the chemical composition of surfaces of cleaved and polished samples. Therefore, the chemical identity of features imaged as point defects is difficult to establish.<sup>5,7</sup>

These problems prompted several successful studies of thin insulating films grown on conducting substrates.<sup>12-14</sup> These systems are free from charging problems and allow, in principle, a much better control of the surface chemical structure. However, the film structure depends on the substrate and conditions of growth,<sup>13</sup> and the film surface is not generally representative of the surface of a bulk sample of the same material.<sup>15</sup> This, nevertheless, does not make these studies less interesting because by choosing growth and imaging conditions one can focus on different aspects, such as the growth mode,<sup>14</sup> the atomistic structure of films,<sup>3</sup> and the mechanisms of growth nucleation.<sup>16</sup> Each of these aspects is of great importance for an understanding of the structure and properties of metal-insulator interfaces, mechanisms of film growth, and conditions of DFM imaging of insulators and insulating films on metals with atomic resolution.

Following this approach, properties of NaCl films grown on the Cu(111) surface were recently studied using a combi-

nation of low-energy electron diffraction (LEED) and DFM. Growth modes, orientation, and lattice constants of ultrathin films were revealed,<sup>11</sup> and atomic resolution at step edges was demonstrated.<sup>3</sup> The aim of the present work is to combine experimental data with atomistic modeling to achieve a better understanding of the mechanism of contrast formation in DFM images, and to obtain more information about the tip and film structures.

To model DFM imaging one should be able to accurately represent the tip-surface interactions and simulate the oscillations of the cantilever under the influence of these interactions. The second problem was studied in detail,<sup>17-19</sup> and analytical<sup>20</sup> and numerical<sup>8</sup> methods have been suggested for calculations of the cantilever's oscillatory behavior under the influence of the tip-surface interaction. However, there is no such consensus in calculations of the tip-surface interaction itself. The difficulties involved in modeling these complex systems mean that techniques have been chosen based on their suitability for a specific tip-surface combination. For example, studies on the Si(111) surface<sup>21</sup> were performed using *ab initio* simulation, so that the importance of dangling bonds in contrast formation could be modeled. On much more strongly ionically insulating surfaces, interatomic potentials were successfully applied to model imaging.<sup>8</sup>

In some other studies the main contributions to the interaction between an atomic force microscopy tip and a surface were analyzed in great detail,<sup>22</sup> but as yet the link between experimental images and theoretical models of the tip-surface interaction remains elusive. In light of this it is crucial to try and model specific experimental systems, especially those with atomically resolved features. If the interaction responsible for resolving an atom can be understood, it should be much easier to develop a general model for interpretation of DFM images. In this paper we explain the nature of enhanced contrast at step edges and kink sites, and, by combining the experimental data with theory, estimate the film thickness. We discuss the shape and chemical

structure of the tip, and the mechanism of damping during DFM imaging.

The plan of the paper is as follows. In Sec. II we discuss the experimental setup used for DFM studies of the NaCl film grown on the Cu(111) surface. Then we present DFM images and discuss their properties. The theoretical model is described in Sec. IV, and the results of an atomistic modeling of DFM imaging of the NaCl film on metallic substrate are presented in Sec. V. We discuss the results of this work and the directions of future studies in Sec. VI.

## II. EXPERIMENTAL SETUP

The experimental results presented in this study were obtained by DFM. In this noncontact type of force microscopy, the interaction between a sharp tip and the sample changes the parameters of the cantilever oscillations. The surface image is recorded by analyzing the dynamic properties of a cantilever bearing the tip as it scans the surface. The cantilever is excited to oscillate at its fundamental eigenfrequency with a constant amplitude by shaking the fixed end of the cantilever with a piezoactuator. In a phase-locked loop, the detected frequency of the cantilever oscillation is used for its excitation. Therefore, any frequency shift induced by the tip-sample interaction is tracked by the system. Attractive forces between the tip and sample result in a reduction of the eigenfrequency of the cantilever oscillation. By regulating the height of the cantilever above the surface to keep the frequency shift constant during scanning, one obtains a surface image which resembles a surface of constant tip-sample interaction.<sup>20</sup> The relation between the frequency shift and tip-sample forces is discussed in detail in Sec. IV.

The amplitude  $A_{exc}$  of the excitation voltage applied to the piezoactuator is regulated so that a constant amplitude  $A_0$  of the tip oscillations is maintained. Any energy dissipation in the course of the tip-sample interaction, which damps the cantilever oscillation, results in an increase of  $A_{exc}$ . Therefore,  $A_{exc}$  is often referred to as a damping signal. A spatially resolved image of damping of the cantilever oscillation can be measured by recording the excitation amplitude  $A_{exc}$ . The excitation amplitude  $A_{exc}$ , which is needed to compensate for the internal friction, can be used to relate the recorded signal  $A_{exc}$  to the dissipated energy. In spite of recent efforts<sup>23–29</sup> a quantitative understanding of  $A_{exc}$  measurements is not straightforward due to both technical problems and the absence of a clear understanding of the dissipation mechanism.

The instrument used in this study is a home-built multifunctional ultrahigh-vacuum scanning force microscope.<sup>30</sup> The oscillation frequency and amplitude and tip-sample distance are controlled by a fully digitized device.<sup>31</sup> The experiments were performed using a single-crystal rectangular silicon cantilever with a spring constant of 26 N/m and a resonance frequency of 158271 Hz. The quality factor  $Q$  of this cantilever was 24000. An oscillation amplitude of 1.8 nm was kept fixed during the experiments, resulting in an energy loss of  $\Delta E_{int} = 70$  meV per oscillation cycle. The frequency shift was set to  $\Delta f = -128$  Hz while recording topography images. The pyramidal silicon tip carried a native oxide layer. Before recording the images presented in this paper, the tip was several times in contact with the NaCl/

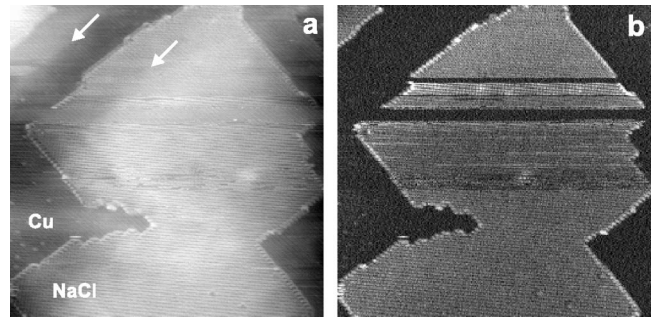


FIG. 1. (a) Topography and (b)  $A_{exc}$  images of a NaCl island on Cu(111). The image size is  $35 \times 35$  nm<sup>2</sup>. The two arrows indicate a weak shadow effect in the topography which is characteristic of a double tip. Note that the double tip does not affect the  $A_{exc}$  image.

Cu(111) sample, thereby destroying the film locally. For these reasons the chemical composition of the tip apex is not known exactly. However, it is most probably oxidized silicon possibly with traces of NaCl.

The copper substrate exhibits 50–250-nm large atomically flat terraces with single sulfur impurities as the only significant contamination. Ultrathin films of NaCl on a clean Cu(111) substrate were prepared by evaporation of NaCl from a Knudsen cell onto the clean Cu(111) surface. The procedure as well as the growth modes of this system were described in a recent publication.<sup>11</sup>

## III. EXPERIMENTAL RESULTS

The DFM images presented in Fig. 1 show a NaCl island on Cu(111) with rectangularly oriented edges. The NaCl has a higher contrast than the Cu substrate, and island edges have a higher contrast compared to the terrace and show an atomically resolved corrugation. In the topography image, the kink sites stick out even more than normal edge sites. The bright dots which appear on the copper substrate are most probably single sulfur impurity atoms.

All images which showed periodicity on an atomic scale were analyzed by means of Fourier analysis. In all cases, a fourfold symmetry was found with a nearest-neighbor distance varying between about 0.36 and 0.42 nm. This scattering can be attributed to mechanical and thermal drift of the piezoactuators, as well as to nonlinearities in the piezo characteristic when scanning with some offset from the relaxed position. The expected distance between nearest-neighbor sodium or chlorine ions in NaCl is about 0.4 nm. Based on this distance correspondence and on the shape of NaCl islands, we believe that they expose the (001) NaCl surface. This conclusion is supported by the LEED spectra measured on these islands.<sup>11</sup> However, only one type of lattice site is imaged as a protrusion in DFM, which is confirmed by our modeling presented below. Similar results have been obtained on other binary compounds.<sup>6,12,32</sup>

Figure 2 shows magnified topographic (a) and  $A_{exc}$  (b) images of an area which we have chosen for further discussions. The individually imaged kink sites demonstrate the resolution of DFM. It is impossible to tell whether the maxima in observed contrast really correspond to average positions of the Na or Cl. The kink and corner sites which terminate the island exhibit several characteristic shapes.

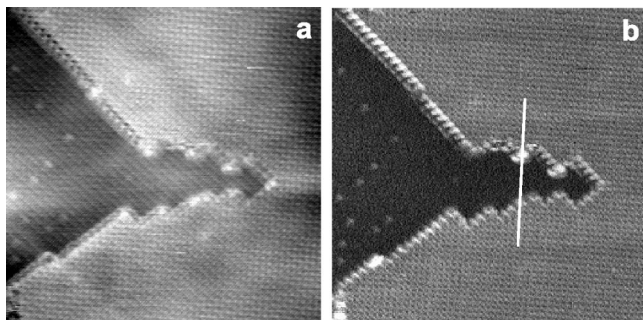


FIG. 2. (a) Enlarged topography and (b)  $A_{exc}$  images of the area mapped in Fig. 1. The image size is  $18 \times 18 \text{ nm}^2$ .

Since both cation- or anion-terminated kink sites may occur in the course of the NaCl island growth, such characteristic shapes may act as fingerprints for the identification of kink site types.

Several instabilities in the tip constitution were detected. These show up as contrast changes in the topography, but do not prevent a stable regulation of the tip-sample distance. For example, during a repeated scanning of the area mapped in Fig. 2, a tip change occurred which is documented in Fig. 3. When passing the kink site in the lower left part of the frame, the tip changed, resulting in a significant change in the contrast in the topography image and a contrast enhancement in the  $A_{exc}$  image. After scanning two-thirds of the image, the tip again changed its composition, and at this time the original contrast in both signals was re-established. Although the characteristic shape of the different kink sites was affected by the tip change, each type of the kink site retained a distinguishing appearance.

The average height difference between the Cu substrate and the top of the NaCl island in the DFM images is around 0.07 nm, which is unrealistically small for a distance between an adsorbed NaCl layer and a Cu surface. In fact, DFM does not yield the real thickness of adsorbed clusters or layers if adsorbed and substrate materials are significantly different, e.g., NaCl on Cu. This is due to the fact that DFM probes the force field, which is very different for ionic materials and metals. Therefore, for given parameters of the cantilever oscillations and frequency change, DFM may record a substrate image at a “height” similar to that of the

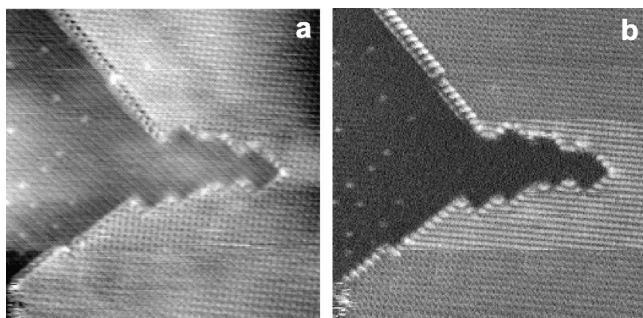


FIG. 3. (a) Topography and (b)  $A_{exc}$  images of a NaCl island on Cu(111). The tip changes after one-fourth of the scan, thereby changing the contrast in topography and increasing the contrast in  $A_{exc}$ . After two-thirds of the scan, the contrast from the lower part of the images is reproduced, indicating that the tip change was reversible. The image size is  $18 \times 18 \text{ nm}^2$ .

adsorbed layer. This means that the detected change in the equilibrium cantilever position as the tip passes over the NaCl cluster edge does not directly reflect the step height.<sup>33</sup> It can correspond to the real height only on a similar substrate. To further illustrate this point, in a topography image of a NaCl island on top of a NaCl terrace,<sup>33</sup> the observed step height is close to the expected value of 0.28 nm, and it exhibits corrugation on the atomic scale on both the upper and lower terraces.

We note a qualitative agreement between the characteristic features of DFM images of NaCl islands in Figs. 2 and 3, and in images of NaCl islands on NaCl terraces recorded with a different experimental setup:<sup>33</sup> island edges in these images look “brighter” than their inner parts, and kink sites seem to be even brighter than edges. The protrusion of step and kink sites is found to be characteristic of NaCl step edges rather than of the underlying substrate. The observed differences in the corrugation height and in the relative extension and appearance of step and kink sites can be attributed to different tip atomic structures. The dependence of contrast on tip structure is clearly demonstrated in Fig. 3.

To characterize the irregular sites of the NaCl film, we have analyzed cross sections of the three-dimensional data represented in experimental images. Figure 4(a) is another image of the area mapped above. The two parallel cross sections along the (100) direction across the steps ( $M$  and  $N$ ) are plotted in Fig. 4(b). The two sections  $M$  and  $N$  were taken through two parallel rows of atoms separated by the nearest-neighbor distance, which is about 0.28 nm. Section  $M$  crosses the step edge at a site imaged as bright, whereas section  $N$  crosses over a site seen as dark. Two different images are compared, one presented in Fig. 4(a) and the one presented in Fig. 3(a) where the contrast is significantly improved after the tip change. Sections  $M$  and  $N$  are made through the same geometric sites in both images. They are aligned in such a way that zero on the abscissa corresponds to the geometrical edge of the NaCl island indicated by the arrow in Fig. 4(a). In spite of the difference in the tip structure the two cross sections exhibit similar features. The atomic corrugation on the terrace in the image shown in Fig. 4(a) is found to be around 0.015 nm, while the step site in section  $M$  protrudes by about one-third of the corrugation height. The image shown in Fig. 3(a) exhibits a more regular and stronger corrugation which demonstrates only a marginal increase at the step. In contrast, section  $N$  exhibits a characteristic dip at the step site in both images.

The three cross sections  $L$  shown in Fig. 4(c) run along the (110) direction across the same kink site [shown in Fig. 4(a)], and are taken from three different images shown in Figs. 2, 3, and 4. The image corrugation on the terrace does not differ significantly from that along the (100) direction. This demonstrates the reproducibility of our data even after the tip change in Fig. 3. These cross sections across the kink site exhibit wide peaks which have a corrugation about three times that on the terrace.

A similar analysis can be made for the damping signal. In Fig. 5 we present a cross section through the  $A_{exc}$  data mapped in Fig. 2(b). As indicated in this figure, the section runs over two different kink sites. The zero point of the  $A_{exc}$  axis has been arbitrarily set to the value measured on the copper substrate. We should note that each ion site is imaged

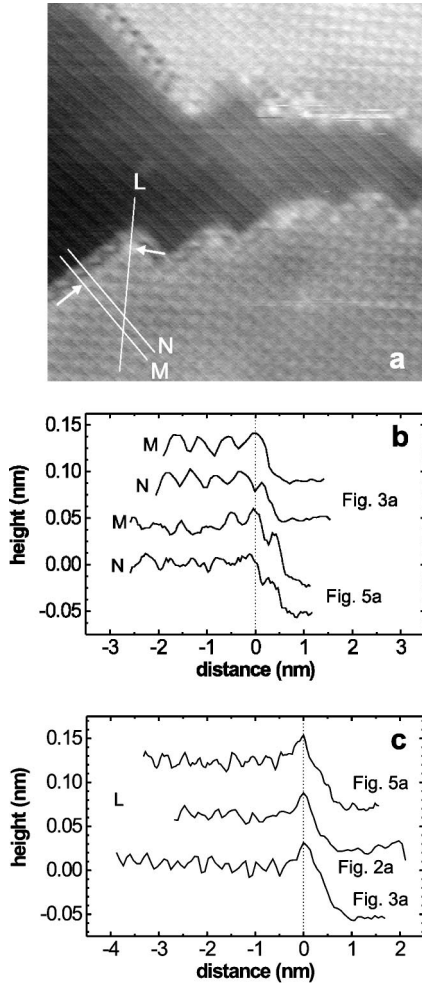


FIG. 4. (a) Topography image of a detail of the area mapped in Fig. 2. The lines mark the cross sections plotted in (b) and (c), and the arrows indicate the distance zero in those cross sections. (b) Parallel cross sections across a step. Section *M* intersects the step at a protrusion, and section *N* in between two protrusions. Note that both sections run along protrusions on the terrace. The sections are taken from different images as indicated. (c) Three cross sections from different images along the same line *L*, cutting a kink site.

by a series of about 3300 oscillation cycles, and that the time constant of the amplitude regulator corresponds to about 300 cycles. Therefore, the measurement of  $A_{exc}$  averages over hundreds of oscillation cycles, but allows detection of varia-

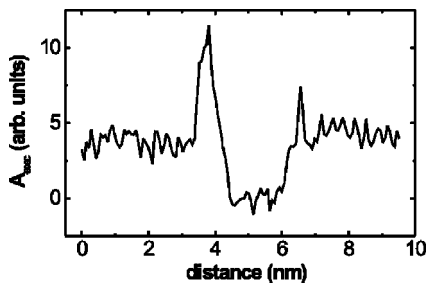


FIG. 5. Cross sections from Fig. 2.  $A_{exc}$  is given in arbitrary voltage units. The variation of  $A_{exc}$  in this cross section corresponds to a power loss which is of the same order of magnitude as the power loss due to internal friction in the cantilever, i.e., 70 meV per oscillation cycle.

tions on the atomic scale. In an attempt to establish a direct spatial correspondence between the two signals, we have studied the match between topography and  $A_{exc}$  on different images and along different directions. We have found that sometimes topography and  $A_{exc}$  are in phase, sometimes they are shifted a little bit in relation to one another, and sometimes  $A_{exc}$  is at a minimum when topography is at a maximum. One explanation for this behavior is that the local contrast formation on the atomic scale depends so much on the atomic tip structure that even the spatial correlation between  $A_{exc}$  and topography is affected by tip changes.

Finally, we should note that although the features in the topography and in the  $A_{exc}$  image are quite similar, there are differences which allow some conclusions about the respective imaging mechanism to be made. First, the characteristic appearance of the NaCl island edges running to the upper right differ from that of edges running to the upper left in both Figs. 2 and 3. This difference can be attributed to an asymmetry in the atomic shape of the tip apex. The step image is essentially a convolution of the tip apex and the step edge, and, with the tip not being a perfect pyramid but an asymmetric cluster, steps running in different directions will be imaged as having slightly different shapes. Second, in the upper right corner of Fig. 1(a), one can note a weak shadow of the island edge which indicates that we were using a double tip, whereby the weak shadow is produced by a tip apex which is less protruding than the one giving the best contrast. The distance to the second tip is about 5 nm. Figure 1(b) does not show a corresponding shadow, indicating that the double tip does not affect the  $A_{exc}$  image. Furthermore, atomic-scale changes of the tip during scanning have a dramatic influence on the contrast of the  $A_{exc}$  signal, while a stable imaging of the topography is still possible. This suggests that the  $A_{exc}$  contrast could be formed by a shorter range interaction than topography. It is also substantially dependent on the composition of the very tip apex. The higher quality of  $A_{exc}$  images is also owed to the fact that  $A_{exc}$  is a measured but not regulated quantity in contrast to the topography signal, which is subject to instrumental drift and regulation noise.

To summarize, DFM images of NaCl islands demonstrate enhanced tip-surface interaction with step edges and kinks. The image features cannot be directly attributed to Na or Cl ions, the thickness of the NaCl island is impossible to measure with DFM, and the contrast in both topographic and  $A_{exc}$  images strongly depends on atomic composition of the end of the tip. In our theoretical analysis presented below, we try to address some of these issues by modeling the experimental setup as accurately as possible. We demonstrate that, combining the experimental data with a realistic theoretical model of DFM, we can make some conclusions regarding the tip material, the thickness of the NaCl island, and the forces involved, and explain the nature of the image contrast.

#### IV. THEORETICAL MODEL

The model used in this study is based on that described in Refs. 8 and 34, so we will only detail the differences in the model used here and briefly outline those parts which are the same. In Sec. IV A we will apply this model to the experi-

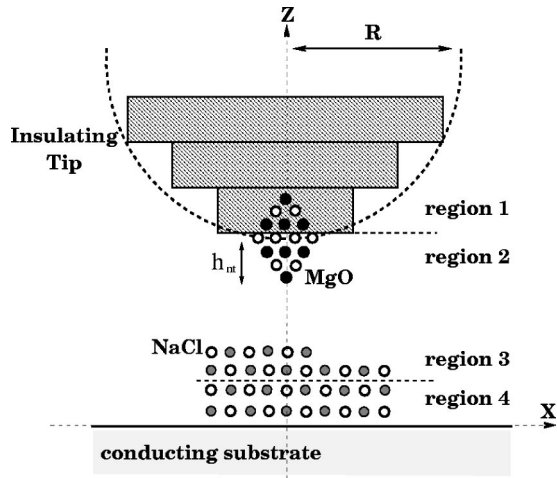


FIG. 6. Schematic picture of the model used here to simulate the interaction between the tip and sample.  $R$  is the effective radius of the macroscopic tip, and  $h_{nt}$  is the protrusion of the nanotip below the macroscopic tip.

mental system described previously and discuss the specific parameters and assumptions used in our calculations.

### A. Tip-surface interaction

In experimental setups, such as that discussed previously, the force can be split into three general components depending on the specific tip-surface combination studied: (i) the *microscopic* chemical force between atoms in the tip and surface, which includes the van der Waals force between ions; (ii) the *macroscopic* van der Waals force between the tip and surface; and (iii) the bias in the system and image forces<sup>34,35</sup> due to polarization of conducting materials. Many studies<sup>8–10</sup> of scanning force microscopy have demonstrated that it is important to model the tip-surface interaction at an atomistic level because surface relaxation and tip contamination<sup>36</sup> by surface and/or ambient atoms has a significant effect on contrast in scanning force microscopy images. This can be seen in the experimental image in Fig. 3, where a tip change at the atomic level causes a dramatic change in the contrast. Therefore, a complete model must include not only an accurate description of these forces, but also an accurate description of the behavior of tip and surface atoms under the influence of these forces.

A schematic diagram of the tip and surface setup used in the calculations is shown in Fig. 6. The doped Si tip has a pyramidlike shape at the macroscopic scale, with a sphere of effective radius of 10 nm at the end. It is very likely to be contaminated by exposure to air, and to be coated by an oxide layer of unknown thickness; therefore, its conduction properties are unknown. The temporary change in contrast in Fig. 3, the dependence of the step image on the scan direction in Figs. 2 and 4, and the possibility of a double tip discussed above shows that there is some sort of nanoasperity at the bottom of the tip which can be contaminated by surface and ambient ions. The importance of a nanoasperity in DFM was also recently discussed in images of a MgO surface.<sup>37</sup>

We performed a study of different possible nanotip models to try and determine which most closely matches the

experimental behavior. First, we found that if the bottom of the tip was flat, i.e., no nanotip, then the interaction with the surface was averaged over several tip ions and no contrast was produced. When a nanotip is included, we found that it must extend significantly beyond the main part of the tip to reproduce the interaction observed in the experiment. Specifically a nanotip of only a few atoms would not atomically resolve the lower terrace. Also, a smaller nanotip would be prevented from getting close enough to the lower terrace for atomic resolution due to the interaction of the main tip with the upper terrace.

Therefore we use a 64-atom MgO cube as a nanotip embedded into the macroscopic tip to reproduce the potential from an oxygen-contaminated or oxidized silicon tip.<sup>36</sup> The cube is orientated so that it is symmetric about the  $z$  axis, with a single oxygen ion at the lowest point of the tip. The difference in imaging of opposite step edges, observed in Fig. 2, can be reproduced by reorienting the tip so that, for example, one cube edge is nearer to the surface than the others. However, this  $z$ -symmetry tip orientation will reproduce the significant interactions involved in imaging effectively.

To integrate macroscopic and microscopic interactions in the same model, we used the following approach. It was shown in previous studies<sup>8,34</sup> that for a locally neutral system, the short-range chemical forces are responsible for atomic resolution. It was also shown that the macroscopic van der Waals and image forces act as a *background attractive force* which is important in terms of reproducing experimentally observed frequency changes, but is independent of the identity of the atom under the tip and does not play a role in atomic displacements. This means that the interactions can be calculated separately, and just combined for the final stages of modeling. In the scanlines shown in Sec. IV B the macroscopic force is included by calculating the image force and macroscopic van der Waals, and then adding them to the microscopic force as a function of tip-surface distance to give the total force, as discussed in Refs. 8 and 34. The distance dependence of the van der Waals force is calculated using the model of a conical tip with a sphere of radius  $R = 10$  nm at the apex, and the method described in Ref. 38.

#### 1. Microscopic forces

The interaction between ions in regions 1–4 in Fig. 6 was calculated using a static atomistic simulation technique as implemented in the MARVIN computer code.<sup>39–41</sup> The calculation is periodic, so that the infinite surface is represented; however, this means large surface unit cells must be used to avoid interactions between tip images in different cells. The nanotip and the NaCl film are each divided into two regions, I and II. In terms of Fig. 6, region I consists of region 2 and the top two layers of the film (region 3), and region II consists of region 1 and the remaining bottom two layers of the film (region 4). The region I ions are relaxed explicitly, while the region II ions are kept fixed. The region II ions represent the interface of the nanotip with the macroscopic tip and the interface of the film with the Cu substrate, neither of which are included atomistically in the model.

Electronic polarization of the ions is implemented via the Dick-Overhauser shell model.<sup>42</sup> Buckingham two-body potentials were used to represent the non-Coulombic interac-

tions between the ions in regions 1–4. The parameters for these interactions are well tested, and are fully described in Ref. 43. To calculate the shell-model contribution to the microscopic force between the tip and surface, we first calculate the total shell-model energy of the system at a range of tip-surface separations, and then differentiate it numerically to find the force as a function of separation. We made sure that the shell-model contribution to the force is completely converged with respect to the size of the periodically translated simulation cell.

### B. Cantilever oscillations

In the last stage of the modeling process we calculate the surface image. For this purpose we simulate the cantilever oscillations under the influence of the tip-surface interaction described in Sec. IV A. The oscillations of a cantilever above each particular surface point are driven by an external force provided by excitations applied to the piezoactuator (see Sec. II). The motion of the cantilever in a force field  $F(x, y, z)$  can be described<sup>8</sup> by the equation of motion

$$\ddot{z} + \omega_0^2 z - \frac{\omega_0^2}{k} F(z+h) = 0, \quad (1)$$

where  $\omega_0$  is the oscillating frequency of the cantilever in the absence of any interaction with the surface,  $k$  is the spring constant of the cantilever, and  $h$  is the equilibrium height of the cantilever above the surface in the absence of interaction. This assumes the DFM is operated at constant amplitude and frequency change. We also assume that any damping is completely canceled by an external force, and that  $F(z)$  does not depend on time.

As the cantilever motion is periodic, we can search for a solution of Eq. (1) in the form of a Fourier series for the oscillator coordinate  $z(t)$ . This produces a system of nonlinear equations for which the approximate first-order solution for the frequency of cantilever oscillations in the presence of the interaction ( $\omega$ ) is obtained as

$$\Omega^2 = 1 - \frac{1}{\pi k A_1} \int_0^{2\pi} F(z+h) \cos(\tau) d\tau, \quad (2)$$

where  $\Omega = \omega/\omega_0$  and  $\tau = \omega t$ . The higher-order terms are very small, and do not affect the results produced by the model. A similar result was derived by Giessibl<sup>4</sup> using perturbation theory and a more specific force expression.

By calculating the force field over a range of characteristic surface points, a map of the tip-surface interaction across the whole surface can be generated. This can then be used with Eq. (2) to produce a corresponding map of the change in the frequency of oscillations over the surface as a function of tip-surface separation. A simulated DFM scanline is then produced by calculating the effective cantilever deflection for a given frequency change.

## V. THEORETICAL RESULTS

### A. Tip structure and film thickness

To further quantify our model, we can use the experimentally observed frequency shift to predict the material of the macroscopic tip and estimate the thickness of the NaCl is-

TABLE I. Comparison of NaCl island contributions to van der Waals force.

Tip type	NaCl layers	Force (eV/Å)
Insulator	1	-0.052
	2	-0.074
Conductor	1	-0.138
	2	-0.195

land. By running the model initially with only the chemical interactions between the oxide nanotip and the island, we find that about an additional  $-0.05$  eV/Å background attractive force was needed at characteristic scanning height ( $h_{sc} \sim 0.47$  nm) to reproduce the 128-Hz frequency change observed in experiment. We can then use this number to infer the material of our macroscopic tip and the film thickness by directly calculating the macroscopic and image interactions for different possible setups. We use Fig. 1 to estimate the size of the NaCl island on the Cu substrate. For a monolayer coverage it contains about 6000 atoms. We then calculate the van der Waals and image interaction between the tip and NaCl island/Cu substrate. In these calculations only the macroscopic part of the tip is considered. This is positioned at  $h_{sc} + h_{nt}$  from the surface, where  $h_{nt}$  is the protrusion of the nanotip (see Fig. 6).

To calculate the van der Waals interaction of the tip with the NaCl island, we use a ‘‘pyramid’’ of square blocks placed on top of each other, as shown in Fig. 6 to represent the observed shape of the tip. Each block consists of atoms arranged in a cubic lattice with a lattice constant of 0.21 nm. The van der Waals interaction is calculated by a direct summation of dispersion interactions ( $C_6/r^6$ ) between the atoms in the blocks and the ions in the NaCl island. We first calculated the number of square blocks needed in our atomistic calculations to converge the van der Waals interaction. This was done by simulating the macroscopic pyramid shape with layers of increasing size. The size of the blocks was chosen to represent an observed effective tip radius of 10 nm. We found that three square slabs (approximately 90 000 atoms) of widths 4, 8, and 12 nm, and each of depth 2 nm, placed on top of each other converged the van der Waals interaction.

In this setup the contribution of the metal substrate to the van der Waals force is negligible.<sup>38</sup> We model insulating and conducting tips by using different dispersion coefficients ( $C_6$ ). For an insulating/oxidized tip we used  $C_6$  parameters for MgO-NaCl (Ref. 43) interactions, and for a conducting tip we used parameters for W-NaCl (Ref. 44) interactions. The results are shown in Table I.

If we now compare these values with the background attractive force needed in our model ( $-0.05$  eV/Å) to reproduce experimental frequency shifts, we see that this interaction can provide all of it. In fact this shows that the macroscopic tip is effectively an insulator, and that the NaCl island cannot be more than one or two layers thick or the background force becomes much too large. If we compare with the image interaction, calculated as in Ref. 34, we find that for an insulating tip the image force between tip and island/substrate would be less than  $-0.01$  eV/Å, compared to about  $-0.11$  eV/Å for a conducting tip. This is again

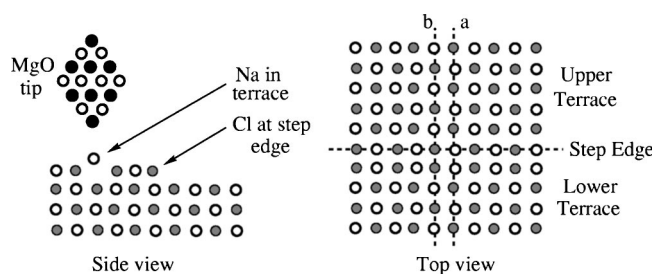


FIG. 7. System schematic for a NaCl step.

consistent with the prediction that the tip is effectively an insulator due to either a thick oxide layer or the poor conduction properties of silicon. These results show that the major contribution to the background force in our model is from the macroscopic van der Waals interaction.

Now that we have established the source of the macroscopic interactions involved, we can calculate the interactions between the small oxide nanotip and a representative 600 atom unit cell (see Sec. IV A), and add a background force which we have demonstrated is mainly due to the van der Waals interaction.

The systems used to calculate the microscopic forces are all setup as shown in Fig. 6, with only the exact structure of the NaCl cell changing between systems. The cells used consist of four layers of NaCl, with the top two layers designated region 3 and the bottom two layers designated region 4, as in Fig. 6. The metal substrate is 0.2 nm below the bottom of the layer, and does not chemically interact with NaCl. A direct modeling of the NaCl-Cu interaction would require an expensive quantum treatment. Instead we use two fixed layers of NaCl to represent the substrate. This is justified by the experimental data presented in Figs. 1–4, which demonstrate very similar qualitative features for both NaCl islands on Cu and on a NaCl film. It also allows us to account for the deformation of the NaCl due to the interaction with the tip, which proved to be important for the understanding of the contrast mechanism.

To keep consistency with the experimental setup (also see Ref. 3), the bias between the tip and substrate was held at 1.0 V in all calculations. This is implemented in the image force calculation, as discussed in detail in Ref. 34. All theoretical scanlines were calculated with an experimental oscillation amplitude of 1.8 nm, a frequency 158 kHz, and a constant frequency change of 128 Hz. The spring constant of the cantilever was  $26 \text{ N m}^{-1}$ .

### B. NaCl step

To calculate the chemical interaction between the nanotip and the edge of the NaCl island, we used a stepped NaCl cell produced by placing a  $5 \times 3 \times 2$  (in terms of an eight atom cubic unit cell) block on top of a  $5 \times 5 \times 2$  block, so that two corners are aligned. A schematic for the calculation cell of this system is shown in Fig. 7. The upper terrace of the step is a good representation of the ideal (001) surface of NaCl, as long as we remain at least two rows from the edge the forces are converged with respect to row choice. However, the ions at the step edge have a coordination of 4, as compared to a coordination of 5 for the terrace ions. This combination al-

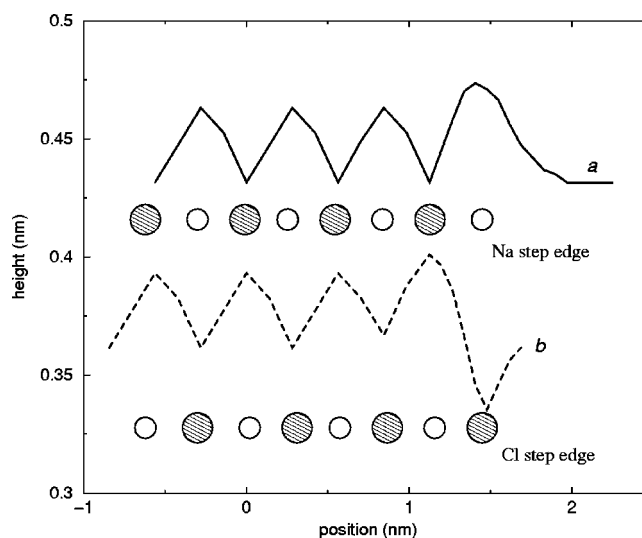


FIG. 8. Simulated scanlines over NaCl step edges. Note that both scanlines are at the same height, but *b* was shifted down for clarity.

lows us to model both the upper terrace and the edge of a NaCl island, features which are atomically resolved in experimental images (Fig. 2).

Figure 8 shows simulated scanlines along the dashed lines labeled *a* and *b* in Fig. 7, beginning on the upper terrace. The schematic atoms in Fig. 8 show the positions of ions in the lattice. The solid scanline *a* in Fig. 8 crossed the step edge over a Na ion, as shown by Fig. 7. However, the first two peaks in the scanline are calculated above an unstepped NaCl film, which effectively represents the ideal (001) surface. This is added to the scanline to show how the interaction on the upper terrace converges to the ideal surface away from the step edge. The periodicity of the microscopic calculations means that there is another step edge on the left-hand side of the cell (looking at the side view in Fig. 7), and calculating the scanline above atoms close to this edge would be unphysical. The axis labeled height in Fig. 8 is a measure of how the center point of the cantilever oscillations changes to keep the frequency change constant. The theoretical model predicts that the tip would come to between about 0.43 and 0.47 nm from the surface.

It is immediately evident from scanline *a* in Fig. 8 that the theoretical model predicts stronger attraction over the Na ions. As shown by the increase in the tip-surface closest distance of approach, they would appear bright in an experimental image. It should be noted that the overall interaction is *always attractive* due to the other forces in the system, and the electrostatic repulsion over the Cl ions just reduces the total attractive force. However, the repulsive chemical force between the tip and chlorine ions is resolved in our model, and the fact that they are represented as dark in experimental images is a matter of convention. The difference between the deflection over terrace Na and Cl ions, i.e., contrast, is about 0.032 nm. This shows that contrast in our model is dominated by the electrostatic interaction between the nanotip and surface ions. The negatively terminated nanotip is attracted to the surface over Na ions and repelled over the Cl ions.

Displacement of ions also plays an important role in the interaction, as at these tip-surface separations surface ions

relax significantly due to the proximity of the tip. Na ions displace by about 0.014 nm toward the tip, and Cl ions displace about 0.006 nm away. Previous studies<sup>8,19</sup> demonstrated that ion displacements create a potential which decays more slowly than the exponentially decaying potential of the ideal surface. This extends the electrostatic potential over the displaced ion: at the scanning height (0.45 nm) the potential from the ideal surface is almost zero, and the extended potential from the displaced ion dominates the electrostatic interaction with the surface.

Figure 8 also shows an increase in contrast (and therefore predicted image brightness) over the Na ion at the step edge; the difference in contrast between the Na ion at the edge and the Cl ion in the terrace along  $a$  is 0.043 nm. The increase in contrast at the step edge has two components: (i) the electrostatic potential at the step edge extends much farther than over the terrace;<sup>8</sup> and (ii) the low coordination of the step-edge ion increases the displacement (step-edge Na displaces by 0.024 nm toward the tip) when the tip is at scanning height, again extending the electrostatic potential.

The dashed line  $b$  in Fig. 8 shows a parallel scanline along  $b$  in Fig. 7. As expected contrast over the terrace ions is the same, about 0.032 nm. However, we now see an increase in contrast to about 0.035 nm over the Na ion just before the step edge, and then the tip moves closer to the surface over the Cl ions at the step edge. This means that the model also gives contrast along the step edge itself; in fact, the difference between deflection over the Cl and Na ions both at the step edge is about 0.07 nm. The scanline behavior over the Cl ion at the step edge is again due to the ion's low coordination, which causes a reduction in the attractive force on the tip. The edge Cl ion displaces by about 0.009 nm away from the tip as it passes the step edge.

The solid scanline  $a$  over the Na step edge in Fig. 8 seems to decay to a constant height after passing the step edge, whereas the dashed scanline first dips over the chlorine ion before rising again as it passes the step. In both cases this is due to the interaction of the side of the tip with the step as it passes, and is a consequence of the specific nanotip we use in the model. This also strongly effects the behavior of the scanlines as the tip passes the step edge and moves to the lower terrace. The strong tip-side-island-edge interaction means that there are large instabilities of tip and edge ions, and the first few rows of the lower terrace cannot be resolved, so they have been omitted from these and all other scanlines. In the current periodic model the island is not large enough to escape the edge interaction and begin to image the lower terrace before the tip starts to interact with the step edge of the next island image. Since in the specific experiment being modeled here there is no lower terrace of NaCl, we did not perform further calculations with a larger island. However, this type of interaction behavior near the edge can also be seen in the scanlines in Fig. 4, where sections  $M$  and  $N$  both show a shoulder beyond the step edge due to an interaction with the side of the nanotip. This confirms our assertion that a protruding nanotip is a real feature of DFM tips in experiments demonstrating atomic resolution.

Figure 8 demonstrates that the theoretical model predicts an increase in contrast at and near the step edge. This would

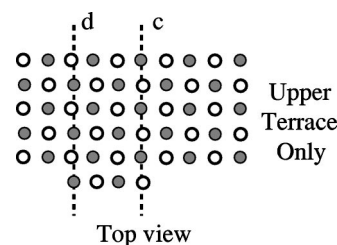


FIG. 9. System schematic for a NaCl kink.

translate to an increased brightness in experimental images along the step edge and along the next row parallel to the edge.

### C. NaCl kink

To model the interaction of the tip with kink sites, we used a unit cell which was produced by removing six atoms from the step edge, creating a double kink site. A schematic diagram of the upper terrace of system is shown in Fig. 9. The kink atoms have a coordination of 3, as compared to 4 at the step edge and 5 in the terrace itself. This allows us to model the interaction over the kink and corner sites which can be seen atomically resolved in experimental images (Fig. 2).

Figure 10 shows simulated scanlines along the dashed lines  $c$  and  $d$  in Fig. 9. The schematic atoms in Fig. 10 show the positions of ions in the lattice. The solid line is a scanline along  $c$  over a Na kink, as shown in Fig. 9. Again the contrast on the terrace ions is the same, about 0.032 nm. Scanline  $c$  also shows an increase in contrast over both the Na ion at the kink site and the next Na ion along the scanline. Over the kink ion the contrast is about 0.062 nm, and over the next Na ion it is about 0.035 nm. This much more delocalized increase in contrast around the kink site is due to the very low coordination of the kink ion.

This causes both the kink ion itself and its nearest neighbors to be very susceptible to relaxation when the tip is in proximity. The Na ions near the kink site all displace toward the tip much more easily than terrace ions, causing an increase in force on the tip near the kink site. The kink ion

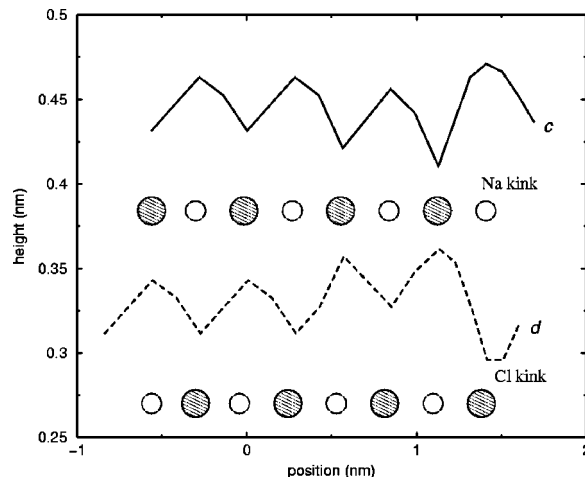


FIG. 10. Simulated scanlines over different kink sites. Note that both scanlines are at the same height, but  $d$  was shifted down for clarity.

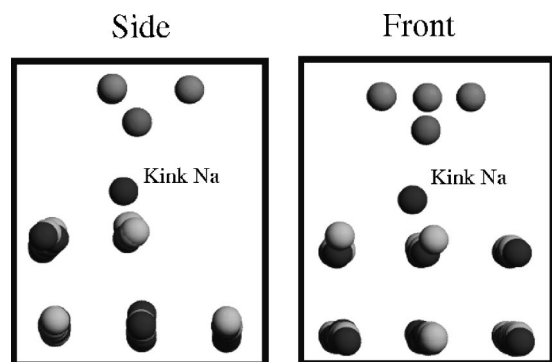


FIG. 11. Simulation snapshots from the side and front showing atomic displacements as the tip passes the kink site sodium ion (labeled kink Na). The snapshots are taken from the simulation of scanline *c* in Fig. 9.

itself displaces upwards by 0.025 nm and the nearest Na ion along *c* by 0.018 nm. A simulation snapshot of the tip passing over the kink site in Fig. 11 clearly shows the large disturbance of all ions around the kink.

The dashed line *d* in Fig. 10 shows a parallel scanline along the line *d* in Fig. 9. This allows us to see the interaction over a Cl kink and also over the Na ion directly behind the kink site. The same behavior as seen in the Na kink scanline is demonstrated; there is a general increase in contrast over Na ions near the kink site. The contrast rises to 0.035 nm over the Na ion directly behind the Cl kink ion, before the deflection falls rapidly as it passes over the kink. The Na ion is displaced by 0.024 nm and the Cl ion at the kink site moves 0.009 nm away from the tip, but all the atoms near the kink site experience strong displacements.

We can clearly see from the kink scanlines that the theoretical model predicts that kink sites would be the brightest feature in a DFM image, and that the Na kink ion would be bright. By comparing several theoretical scanlines we can also see that the much less localized interaction predicted by the model over the kink site would produce a wider area of bright contrast in an image than for terrace and step-edge ions. This corresponds well with the experimental images shown in Figs. 1–4.

#### D. Cation-terminated tips

To study the effect of the chemical identity of the tip apex on the results, we also performed calculations using a tip terminated by a positive  $\text{Mg}^{2+}$  ion and an  $\text{OH}^-$  group. This simulates the situation where the original tip has been contaminated by a positive ion from the surface or from the environment; for example, a water molecule could dissociate on the tip. This also simulates the case where the original uncontaminated tip is terminated by a cation, a situation which cannot be ruled out at present. Both scans in this section were taken along line *b* in Fig. 7.

##### 1. Mg-terminated tip

By reversing the orientation of the MgO cube simulating the nanotip, we can model scanning of the surface with an equally but oppositely charged apex ion. All other parameters are kept the same as previously.

The scanline labeled Mg in Fig. 12 clearly shows that the

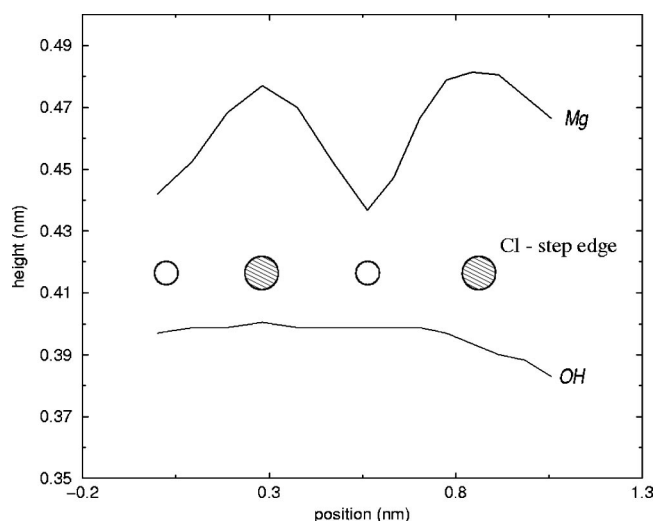


FIG. 12. Simulated scanline over the chlorine step site with Mg- and OH-terminated tips. As previously, scanline OH has been shifted down for clarity.

contrast with an Mg-terminated tip is now dominated by the attractive electrostatic interaction between the Mg at the end of the tip and the Cl ions in the terrace. The magnitude of contrast on the terrace is 0.035 nm, which is a slight increase in comparison with the oxygen-terminated tip. We also again see an increase in contrast to 0.044 nm over the step edge due to the low coordination of the edge ion. However, chlorine ions are more resistant to relaxation, displacing by only 0.019 nm compared to 0.024 nm for the Na ion, so the relative increase in contrast over the step is smaller than scans with an O tip.

##### 2. OH-terminated tip

In this setup the oxygen at the end of the original MgO tip is replaced by a hydroxyl group, and another hydroxyl group is added to the opposite side of the tip to keep it neutral. The electrostatic potential gradient from this OH apex is very similar to the potential gradient<sup>36</sup> from a silicon tip contaminated by a hydroxyl group.

The scanline labeled OH in Fig. 12 shows very different behavior from all the previous tip setups. As for the Mg-terminated tip, ostensibly the attractive electrostatic interaction between the hydrogen at the end of the tip and the chlorine ions in the terrace is the source of contrast. However, the magnitude of contrast is only 0.004 nm, almost an order of magnitude less than with the Mg- and O-terminated tips. This is because at a distance of about 0.48 nm the interaction between the hydrogen and Na and Cl ions is more or less the same, as has been shown in previous studies on contact atomic force microscopy.<sup>40</sup> There is no contrast at all over the ions near the step edge, and the contrast actually decreases rapidly as the tip passes the step edge. This occurs because at the step edge the hydrogen atom interacts with less ions for a given radius than over the terrace. Also, the simulation shows no relaxation of the step-edge ion due to the tip.

## VI. DISCUSSION

This paper presents atomically resolved DFM images of step and kink sites at an ionic surface. The special role of

these sites in adsorption, catalysis, growth, and spectroscopic properties of surfaces is well recognized.<sup>45–49</sup> This role is attributed to changes in the Coulomb potential, charge distribution, and electronic energies at low-coordinated sites with respect to the bulk properties. In this study we were able to measure how these changes affect the interaction of step and kink sites with a DFM tip. The experiment shows that local variation of damping also yields high-quality contrast, and that damping exhibits more short-range character than frequency shift. The experimental results and theoretical modeling systematically demonstrate the enhanced interaction of step and kink sites of one kind with the tip. Combining the experimental and theoretical results we arrive at the following conclusions.

(1) From the orientation of edges, alternating signs of kink sites, and lattice spacing, we conclude that the NaCl islands grown on Cu(111) expose their (001) surface. This agrees with our LEED measurements on these samples.<sup>11</sup> The growth mode of NaCl on Cu(111) is similar to that observed for NaCl on the Al(111) (Ref. 12) and on Ge surfaces<sup>14</sup> at room temperature. A completely different growth pattern of NaCl was recently obtained at low temperature on a Cu(211) surface where thin chainlike NaCl islands were observed by scanning tunneling microscopy (STM).<sup>13</sup> From our data we can conclude that the NaCl islands grown at room temperature on Cu(111) are terminated by a few-nm-long (100) edges. Visual analysis of kink and corner sites suggests that there could be more kinks of one sign than another.

Our DFM measurements alone cannot determine the thickness of NaCl islands. The theoretical analysis suggests that there can be no more than two layers of NaCl. From these data we cannot conclude whether islands grow by assembling NaCl molecules adsorbed flat on the surface, or alternating molecules adsorb perpendicular to the surface.

(2) The results suggest that the tip used in this study is effectively an insulator. The surface of the tip is rough on the nanoscale, and one of the features at the tip end serves as a main nanotip. The image features suggest that another nanoasperity which serves as a second tip is located about 5 nm away from the main one. To reproduce experimentally observed contrast, the nanotip must have a strong electrostatic field which, as demonstrated in Ref. 36, could be generated by a polar group at the tip apex or by an oxide. Our results show that a tip terminated by OH<sup>−</sup> cannot produce the experimentally observed contrast. The results presented in Fig. 3 suggest that the tip can also temporarily trap some surface ions.

(3) The theoretical analysis demonstrates that at long range the tip-surface force is mainly due to the van der Waals interaction. The characteristic scanning tip-surface

distance is predicted to be about 0.43–0.47 nm (with ion instabilities occurring below about 0.42 nm). The contrast in the image is determined by the chemical interaction between the tip and surface ions at this distance. This interaction dominates the forces at short range, and leads to a considerable displacement of surface ions from their ideal sites.

(4) Our modeling predicts that contrast in DFM images corresponds to the average positions of surface ions. Although our tip-surface model is idealized, the contrast mechanism does not allow any other plausible explanation for observed experimental contrast. The increase in contrast (and therefore predicted image brightness) over the step edges and kinks is due to the lower coordination of the step-edge and kink ions. It has two components: (i) the electrostatic potential over the low coordinated sites extends much farther than over the ideal terrace; and (ii) the low coordination of the ions increases their displacements due to the interaction with the tip. These two effects mainly determine the electrostatic interaction with the tip at scanning height.

It is interesting to note that STM experiments on thin films of NaCl on Al(111) by Hebenstreit *et al.*<sup>12</sup> also observed enhanced contrast at step and kink sites. Our results suggest that the tip interaction with these sites could be one of the reasons for this enhanced contrast.

The successful simulation of atomic-resolution DFM reported in this paper motivates further studies in this field. An extension of the simulation toward dissipative interactions would close a gap between experiment and theoretical description. On the experimental side, a further stabilization and noise reduction of the imaging process is highly desirable. This may be obtained in low-temperature experiments and with sophisticated electronic feedback systems. Additionally, a quantitative understanding of DFM could be improved using a tip well defined on the atomic scale, as shown in experiments for metal tips.<sup>50</sup> With these ideas in mind, we believe that an accurate quantification of local interactions with true atomic resolution is within the grasp of DFM studies.

#### ACKNOWLEDGMENTS

We are grateful to A. Baratoff for stimulating discussions, and to H.-J. Güntherodt for continued support. Furthermore, we would like to thank M. Reichling, C. Barth, and R. W. Grimes for valuable comments, and A. L. Rohl for help with the MARVIN code. A. S. Foster and L. N. Kantorovich are grateful to the EP-SRC for financial support. The Basel group acknowledges financial support from the Swiss Priority Program MINAST, the Kommission für Technologie und Innovation, and from the Swiss National Foundation for Scientific Research.

<sup>1</sup> *Proceedings of the First International Workshop on Noncontact Atomic Force Microscopy*, edited by S. Morita [Appl. Surf. Sci. **140**, (1999)].

<sup>2</sup> *Proceedings of the Second International Workshop on Noncontact Atomic Force Microscopy*, edited by R. Bennewitz [Appl. Surf. Sci. **157**, (2000)].

<sup>3</sup> R. Bennewitz, M. Bammerlin, M. Guggisberg, C. Loppacher, A. Baratoff, E. Meyer, and H.-J. Güntherodt, Surf. Interface Anal. **27**, 462 (1999).

<sup>4</sup> F. J. Giessibl, Science **267**, 68 (1995).

<sup>5</sup> M. Reichling and C. Barth, Phys. Rev. Lett. **83**, 768 (1999).

<sup>6</sup> M. Bammerlin, R. Lüthi, E. Meyer, A. Baratoff, M. Guggisberg,

- C. Gerber, L. Howald, and H.-J. Güntherodt, *Probe Microsc.* **1**, 3 (1997).
- <sup>7</sup>A. L. Shluger, A. I. Livshits, A. S. Foster, and C. R. A. Catlow, *J. Phys.: Condens. Matter* **11**, R295 (1999).
- <sup>8</sup>A. I. Livshits, A. L. Shluger, A. L. Rohl, and A. S. Foster, *Phys. Rev. B* **59**, 2436 (1998).
- <sup>9</sup>S. H. Ke, T. Uda, R. Pérez, I. Stich, and K. Terakura, *Phys. Rev. B* **60**, 11 631 (1999).
- <sup>10</sup>J. Tóbiik, I. Stich, R. Pérez, and K. Terakura, *Phys. Rev. B* **60**, 11 639 (1999).
- <sup>11</sup>R. Bennewitz, M. Bammerlin, M. Guggisberg, C. Loppacher, A. Baratoff, E. Meyer, and H.-J. Güntherodt, *Surf. Sci.* **438**, 289 (1999).
- <sup>12</sup>W. Hebenstreit, J. Redinger, Z. Horozova, M. Schmid, R. Podloucky, and P. Varga, *Surf. Sci.* **424**, L321 (1999).
- <sup>13</sup>S. Fölsch, A. Helms, S. Zöphel, J. Repp, G. Meyer, and K. Rieder, *Phys. Rev. Lett.* **84**, 123 (2000).
- <sup>14</sup>K. Glöckler, M. Sokolowska, A. Soukopp, and E. Umbach, *Phys. Rev. B* **54**, 7705 (1996).
- <sup>15</sup>S. Street, C. Xu, and D. W. Goodman, *Annu. Rev. Phys. Chem.* **48**, 43 (1997).
- <sup>16</sup>J. Venables, G. Haas, H. Brune, and J. Harding, *Epitaxial Growth Principles Appl.* **57**, 570 (1999).
- <sup>17</sup>M. Tsukada, N. Sasaki, R. Yamura, N. Sato, and K. Abe, *Surf. Sci.* **401**, 355 (1998).
- <sup>18</sup>J. P. Aimé, R. Boisgard, L. Nony, and G. Couturier, *Phys. Rev. Lett.* **82**, 3388 (1999).
- <sup>19</sup>A. I. Livshits, A. L. Shluger, and A. L. Rohl, *Appl. Surf. Sci.* **140**, 327 (1999).
- <sup>20</sup>F. J. Giessibl, *Phys. Rev. B* **56**, 16 010 (1997).
- <sup>21</sup>R. Pérez, M. Payne, I. Stich, and K. Terakura, *Phys. Rev. Lett.* **78**, 678 (1997).
- <sup>22</sup>N. Burnham, R. Colton, and H. Pollock, *Nanotechnology* **4**, 64 (1993).
- <sup>23</sup>C. Loppacher, M. Bammerlin, M. Guggisberg, F. Battiston, R. Bennewitz, S. Rast, A. Baratoff, E. Meyer, and H.-J. Güntherodt, *Appl. Surf. Sci.* **140**, 287 (1999).
- <sup>24</sup>M. Gauthier and M. Tsukada, *Phys. Rev. B* **60**, 11 716 (1999).
- <sup>25</sup>A. Abdurixit, T. Bonner, A. Baratoff, and E. Meyer, *Appl. Surf. Sci.* **157**, 355 (2000).
- <sup>26</sup>W. Denk and D. W. Pohl, *Appl. Phys. Lett.* **59**, 2171 (1991).
- <sup>27</sup>U. Dürig, *Surf. Interface Anal.* **27**, 467 (1999).
- <sup>28</sup>T. D. Stowe, T. W. Kenny, D. J. Thomson, and D. Rugar, *Appl. Phys. Lett.* **75**, 2785 (1999).
- <sup>29</sup>B. Gotsmann, C. Seidel, B. Anczykowski, and H. Fuchs, *Phys. Rev. B* **60**, 11 051 (1999).
- <sup>30</sup>L. Howald, E. Meyer, R. Lüthi, H. Haefke, R. Overney, H. Rudin, and H.-J. Güntherodt, *Appl. Phys. Lett.* **63**, 117 (1993).
- <sup>31</sup>C. Loppacher, M. Bammerlin, F. Battiston, M. Guggisberg, D. Müller, H. Hidber, R. Lüthi, E. Meyer, and H.-J. Güntherodt, *Appl. Phys. A: Mater. Sci. Process.* **66**, 215 (1998).
- <sup>32</sup>A. Schwarz, W. Allers, U. D. Schwarz, and R. Wiesendanger, *Phys. Rev. B* **61**, 2837 (2000).
- <sup>33</sup>M. Bammerlin *et al.* (unpublished).
- <sup>34</sup>L. N. Kantorovich, A. S. Foster, A. L. Shluger, and A. M. Stoneham, *Surf. Sci.* **445**, 283 (2000).
- <sup>35</sup>L. N. Kantorovich, A. I. Livshits, and A. M. Stoneham, *J. Phys.: Condens. Matter* **12**, 795 (2000).
- <sup>36</sup>P. Susko, A. Foster, L. Kantorovich, and A. Shluger, *Appl. Surf. Sci.* **144-145**, 608 (1999).
- <sup>37</sup>K. Fukui and Y. Iwasawa, *Surf. Sci.* **441**, 529 (1999).
- <sup>38</sup>C. Argento and R. H. French, *J. Appl. Phys.* **80**, 6081 (1996).
- <sup>39</sup>D. Gay and A. Rohl, *J. Chem. Soc., Faraday Trans.* **91**, 925 (1995).
- <sup>40</sup>A. Shluger, A. Rohl, D. Gay, and R. Williams, *J. Phys.: Condens. Matter* **6**, 1825 (1994).
- <sup>41</sup>A. L. Shluger and A. L. Rohl, *Top. Catal.* **3**, 221 (1996).
- <sup>42</sup>B. G. Dick and A. W. Overhauser, *Phys. Rev.* **112**, 603 (1958).
- <sup>43</sup>R. Grimes, C. Catlow, and A. Stoneham, *J. Phys.: Condens. Matter* **1**, 7367 (1989).
- <sup>44</sup>C. Girard, D. V. Labeke, and J. M. Vigoureux, *Phys. Rev. B* **40**, 12 133 (1989).
- <sup>45</sup>A. L. Shluger, P. V. Sushko, and L. N. Kantorovich, *Phys. Rev. B* **59**, 2417 (1999).
- <sup>46</sup>E. Garrone, A. Zecchina, and F. Stone, *Philos. Mag. B* **42**, 683 (1980).
- <sup>47</sup>E. Stefanovich and T. Truong, *J. Chem. Phys.* **102**, 5071 (1995).
- <sup>48</sup>S. Briquez, A. Lakhlifi, S. Picaud, and C. Girardet, *Chem. Phys.* **194**, 65 (1995).
- <sup>49</sup>J. Heidberg, E. Kampshoff, R. Kühnemuth, and O. Schönekas, *Surf. Sci.* **272**, 306 (1992).
- <sup>50</sup>G. Cross, A. Schirmeisen, A. Stalder, P. Grütter, M. Tschudy, and U. Dürig, *Phys. Rev. Lett.* **80**, 4685 (1998).